

## BIOPHYSICS

# Water-ion permselectivity of narrow-diameter carbon nanotubes

Yuhao Li<sup>1\*</sup>, Zhongwu Li<sup>1,2\*</sup>, Fikret Aydin<sup>3\*</sup>, Jana Quan<sup>1</sup>, Xi Chen<sup>1,4</sup>, Yun-Chiao Yao<sup>1,4</sup>, Cheng Zhan<sup>3</sup>, Yunfei Chen<sup>2</sup>, Tuan Anh Pham<sup>3†</sup>, Aleksandr Noy<sup>1,4†</sup>

Carbon nanotube (CNT) pores, which mimic the structure of the aquaporin channels, support extremely high water transport rates that make them strong candidates for building artificial water channels and high-performance membranes. Here, we measure water and ion permeation through 0.8-nm-diameter CNT porins (CNTPs)—short CNT segments embedded in lipid membranes—under optimized experimental conditions. Measured activation energy of water transport through the CNTPs agrees with the barrier values typical for single-file water transport. Well-tempered metadynamics simulations of water transport in CNTPs also report similar activation energy values and provide molecular-scale details of the mechanism for water entry into these channels. CNTPs strongly reject chloride ions and show water-salt permselectivity values comparable to those of commercial desalination membranes.

## INTRODUCTION

Membrane separations have become critical to the human civilization, and there is, perhaps, no better example of their importance than water purification. As water scarcity becomes more common and communities start running out of cheap available water, they need to supplement their supplies with desalinated water from seawater and brackish water sources (1). Reverse osmosis (RO) processes that use thin-film composite (TFC) membranes to separate water from the ions present in saline feed streams currently dominate this industrial sector. Although TFC membranes in combination with advanced energy recovery devices have been pushing the energy efficiency of RO desalination ever closer to the thermodynamic limits, some fundamental performance issues remain (2). TFC membranes are constrained by the permeability-selectivity trade-offs (3) and often have insufficient rejection of some ions and trace uncharged micropollutants, requiring additional purification stages that increase the energy and capital costs (2, 4). Advanced process modeling indicates that further improvements in the functionality of desalination membranes require improvements in the membrane performance, as defined by the critical figure of merit of membrane's water-salt permselectivity,  $P_w/P_s$  (5).

Biological water channels, aquaporins, provide a blueprint for the structures that offer such increased performance. Their defining feature is an extremely narrow inner pore that squeezes water down to a single-file configuration that enables extremely high water permeability, with the single-channel transport rates exceeding  $10^9$  water molecules per second (6). Aquaporins have excellent selectivity and are able to block the passage of most other solutes, including ions and protons (6). As a result, the projected water/salt permselectivity of a membrane that has a dense array of aquaporin channels assembled in a lipid bilayer could reach  $10^{10}$  to  $10^{13}$  (4). Such standout projected performance precipitated a substantial investment in the develop-

ment of biomimetic membranes for water desalination; however, these materials have yet to realize their potential due to problems with long-term stability and cost (7). Artificial water channels (AWCs), which seek to mimic aquaporin's structure and transport mechanism in synthetic structures, provide a more robust alternative to aquaporins and could overcome these drawbacks and deliver on the promise of biomimetic membranes (7, 8).

Carbon nanotubes (CNTs) represent some of the most promising scaffold structures for AWC development because of the low friction of water on their hydrophobic smooth inner surfaces, which mimic the aquaporin structure (9), and their small diameters that potentially enable strong selectivity. Computer simulations (9–12) and experiments using membranes (13, 14), individual CNT channels (15), or CNT pores in lipid membranes (16) demonstrated enhanced flow through inner channels of CNTs. Previous studies also indicated that small-diameter CNTs should have strong ion selectivity (16, 17). Even though some previous work explored using CNTs for reverse osmosis desalination (18), the extent of the water-salt permselectivity of these pores is not yet known.

We have recently developed CNT porins (CNTPs)—short segments of CNTs that self-insert into lipid bilayers and form AWCs that mimic aquaporin channel functionality and intrachannel single-file water arrangement (16, 19). Here, we use this experimental platform to measure water and chloride ion transport through 0.8-nm-diameter CNTPs using fluorescence-based assays that avoid common artifacts of light-scattering measurements. This methodology allowed us to determine the accurate value of water-salt permselectivity in narrow CNT pores. We also report an activation energy for water transport in 0.8-nm-diameter CNTPs that is significantly lower than the previously reported value (16). Well-tempered metadynamics (WT-MetaD) simulations and hybrid quantum-continuum calculations provide a detailed molecular-scale view of water entering the CNTP channels and support the activation energy values that we report.

## RESULTS

### Permeability and activation energy barrier for water transport in CNTPs

We have characterized water permeability of CNTPs using stopped-flow technique to capture fast kinetics of water efflux from vesicles

<sup>1</sup>Materials Science Division, Physical and Life Sciences Directorate, Lawrence Livermore National Laboratory, Livermore, CA 94550, USA. <sup>2</sup>Jiangsu Key Laboratory for Design and Manufacture of Micro-Nano Biomedical Instruments, School of Mechanical Engineering, Southeast University, Nanjing 211189, China. <sup>3</sup>Quantum Simulations Group, Materials Science Division, Physical and Life Sciences Directorate, Lawrence Livermore National Laboratory, Livermore, CA 94550, USA. <sup>4</sup>School of Natural Sciences, University of California Merced, Merced, CA 94343, USA.

\*These authors contributed equally to this work.

†Corresponding author. Email: pham16@llnl.gov (T.A.P.); noy1@llnl.gov (A.N.)

with CNTPs embedded in their walls [CNTP–large unilamellar vesicles (LUVs)] after those vesicles were mixed with a hypertonic osmolyte solution. A common approach in detecting liposomal volume change is light scattering. However, a complicated relationship between the changes in liposome size and their light-scattering intensity and associated artifacts make quantitative measurements of water flux in these experiments a nontrivial task (4, 20, 21). To avoid these problems, we have used a different approach that relied on self-quenching of a fluorescence dye, carboxyfluorescein (CF), encapsulated in the vesicle's lumen (Fig. 1A) (4, 21–23). We have also incorporated 10% of cholesterol in our lipid bilayer composition to increase the vesicle's stability and suppress long-term content leakage. Control experiments showed that these vesicles were extremely stable with no detectable content leaking from the CNTP-LUVs over a period of 2.5 hours (fig. S1).

Fluorescence intensity of the encapsulated CF dye decayed rapidly after the ca. 200-nm-diameter LUVs and CNTP-LUVs were mixed with the hypotonic osmolyte solution (Fig. 1B and fig. S2A), indicating that the osmotic gradient was driving water rapidly out of the vesicles. When a small number of CNTPs were embedded in the walls of CNTP-LUVs, their volume changed significantly faster (Fig. 1B), indicating that even a small number of CNTPs provided an efficient water transport pathway. The rate of water efflux increased with the increase in the osmolyte concentration and the corresponding driving force. The unitary permeability  $P_w$  of 0.8-nm-diameter CNTPs determined from these measurements,  $(2.30 \pm 0.10) \times 10^{-13} \text{ cm}^3/\text{s}$ , falls in the same range (albeit slightly lower) as the values that we previously reported on the basis of light-scattering measurements (16). Notably, this value is higher than the unitary permeability of aquaporins (Fig. 1C), in agreement with the previous simulation predictions and experimental reports (10, 16, 20).

Molecular dynamics (MD) simulations indicate that the single-file water arrangement in the CNTP channel is the main reason for its very high water permeability (10). A survey of other fast water membrane transporters with similar water molecule arrangements in the channel indicates that another hallmark of this mode of transport is an activation energy,  $E_a$ , value in the range of 4 to 6 kcal/mol, i.e., a value that is the same order of magnitude as the activation energy for the self-diffusion of water (6, 24, 25). To test whether this assumption

also holds true for CNTPs, we measured their water permeability as a function of temperature (Fig. 2). To ensure bilayer stability and to avoid artifacts, we also restricted the temperatures used for the measurements to a small range around room temperature (Fig. 2, A and C). Control experiments indicated that dioleoyl phosphatidylcholine (DOPC) LUVs had a rather large  $E_a$  value of  $16.1 \pm 0.2 \text{ kcal/mol}$  for their background water permeability (Fig. 2B), which was also close to the values previously reported in the literature (23, 26). In contrast, measured  $E_a$  values for water transport through CNTPs (Fig. 2D),  $5.3 \pm 1.0 \text{ kcal/mol}$ , were significantly lower, falling in the range of the transport barrier values for the single-file water channels. It also was significantly lower than the values that we have reported previously (16). Control experiments showed similarly low  $E_a$  values for water transport through the CNTPs synthesized by sonication in pure DOPC or in DOPC/cholesterol mixture (fig. S5), indicating that the lipid composition used to solubilize CNTPs does not influence water flow.

### Computational modeling of water entry into CNTPs

To get more insights into the mechanism of water entry into the CNTPs, we also carried out WT-MetaD simulations (27) with classical force fields to probe the activation energy for water transport into the CNTP channel (Fig. 3A) (see Materials and Methods for details). Computed potential of mean force (PMF) of water transport through the CNTP (Fig. 3B) along the minimum free energy path derived from the two-dimensional (2D) PMF (Fig. 3C) yields a low activation energy of ca.  $3.0 \pm 0.5 \text{ kcal/mol}$ . We also calculated the activation energy by using a hybrid quantum-continuum approach, where the CNTP and a permeated water molecule were explicitly treated by density functional theory (DFT), and the rest of the liquid was described by an implicit solvation model (see Materials and Methods). This hybrid quantum-continuum calculation yields a slightly larger value for the activation energy of 4.8 kcal/mol (Fig. 3D), which shows an even better agreement with the  $E_a$  value obtained in our experiment. Significantly, both modeling approaches point to a low activation energy for water transport through a narrow CNTP channel, consistent with other computational studies (28) and our experimental results.

Our WT-MetaD simulations also provide insights into the molecular-scale mechanism of water entry into the CNTPs (Fig. 3,

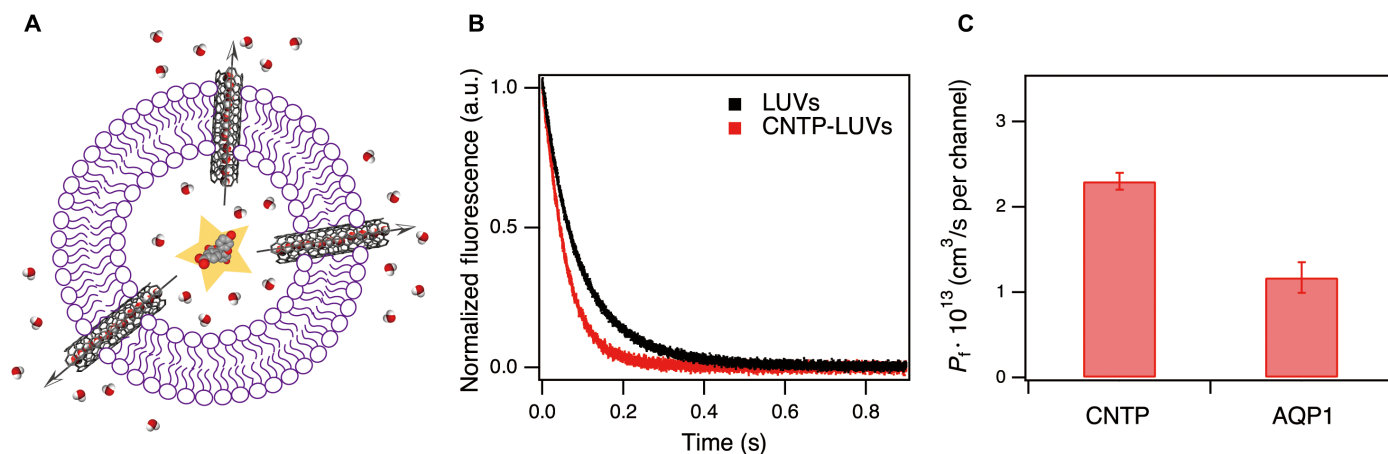


**Fig. 1. Water permeability of CNTPs.** (A) Schematics of dye-encapsulating liposome exposed to hypertonic buffer upon mixing; the escape of water causing vesicle shrinkage and responsible for self-quenching of encapsulated dyes. (B) Representative normalized CF fluorescence curves from the stopped-flow water transport measurements (CNTP-LUVs contained, on average, 16 CNTPs per vesicle). a.u., arbitrary unit. (C) Comparison of the unitary water permeabilities of CNTPs and aquaporin 1 (AQP1) (22).

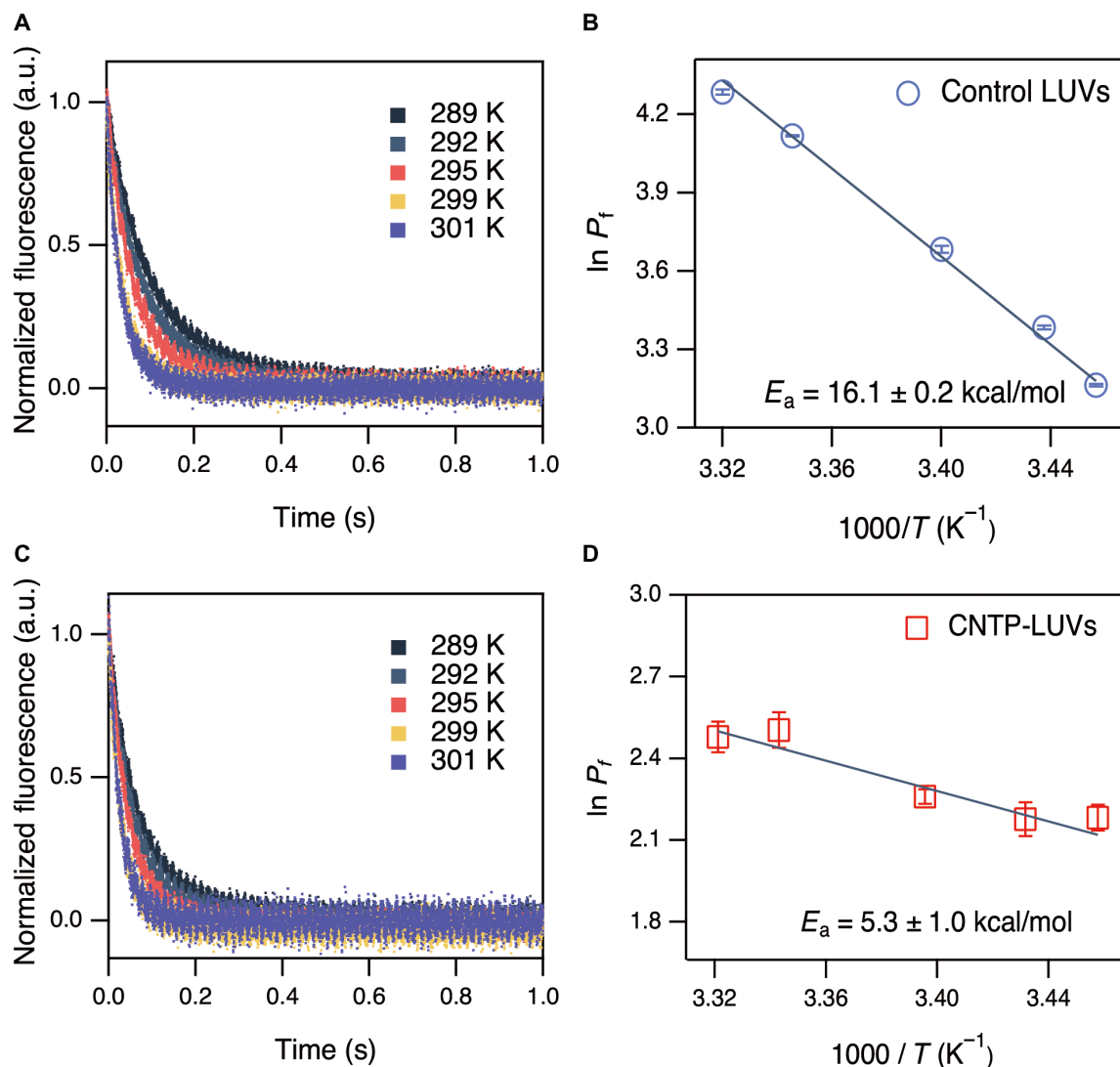


**Fig. 2. Water transport activation energy in CNTPs.** (A) Normalized fluorescent curves indicative of water transport across DOPC membranes at five different temperatures. (B) Arrhenius plots of the water permeability for DOPC LUVs, with corresponding activation energies indicated on the graph. (C) Normalized fluorescent curves indicative of water transport across CNTP-embedded DOPC membranes at five different temperatures. (D) Arrhenius plots of the water permeability  $P_f$  (in units of  $\mu\text{m/s}$ ) for CNTP-LUVs after subtraction of the background water permeability for DOPC-LUVs, with corresponding activation energies indicated on the graph.

E and F; see also movie S1). Time evolution trace of the number of the hydrogen bonds around a water molecule entering the nanotube shows that water transport through the CNTP can be split into three stages. First, the molecule partially desolvates in the liquid reservoir [Fig. 3, E (i and ii) and F], starting at about 25 ps after it first approaches the CNT entrance. This stage is followed by the formation of a pseudosolvation shell around the molecule [Fig. 3, E (iii) and F] consisting of oxygen atoms from both the solvent and the COO<sup>-</sup> groups at CNTP entrance, as seen in the simulation between 50 and 125 ps. Last, after 125 ps, the water molecule loses two hydrogen bonds and becomes a part of the single-file water chain in the CNTP interior [Fig. 3, E (iv) and F].

A low activation energy value that we obtained in the experiments and in the simulations is, perhaps, unexpected, given the loss of two hydrogen bonds that accompany water entry into the CNT channel. However, this value can be rationalized by considering that

the strength of a hydrogen bond in bulk water is considerably smaller than the amount of 5.1 kcal/mol that has been reported for an isolated water dimer (29). This value, however, becomes significantly smaller in liquid water after we include the effects of thermal fluctuation and interactions with other water molecules and represents only a fraction of the water hydration free energy of 6.3 kcal/mol (30). Therefore, a value of 6.3 kcal/mol represents an upper limit for the activation energy of water transport through the CNTPs, a conclusion that is consistent with the experimental values and simulation results that we report.

#### Cl<sup>-</sup> anion permeability determination

Ion selectivity of CNTPs is another important parameter that defines their performance in desalination applications. We have previously reported single-CNTP measurements of ion transport that showed that they are strong cation-selective pores because of the presence of

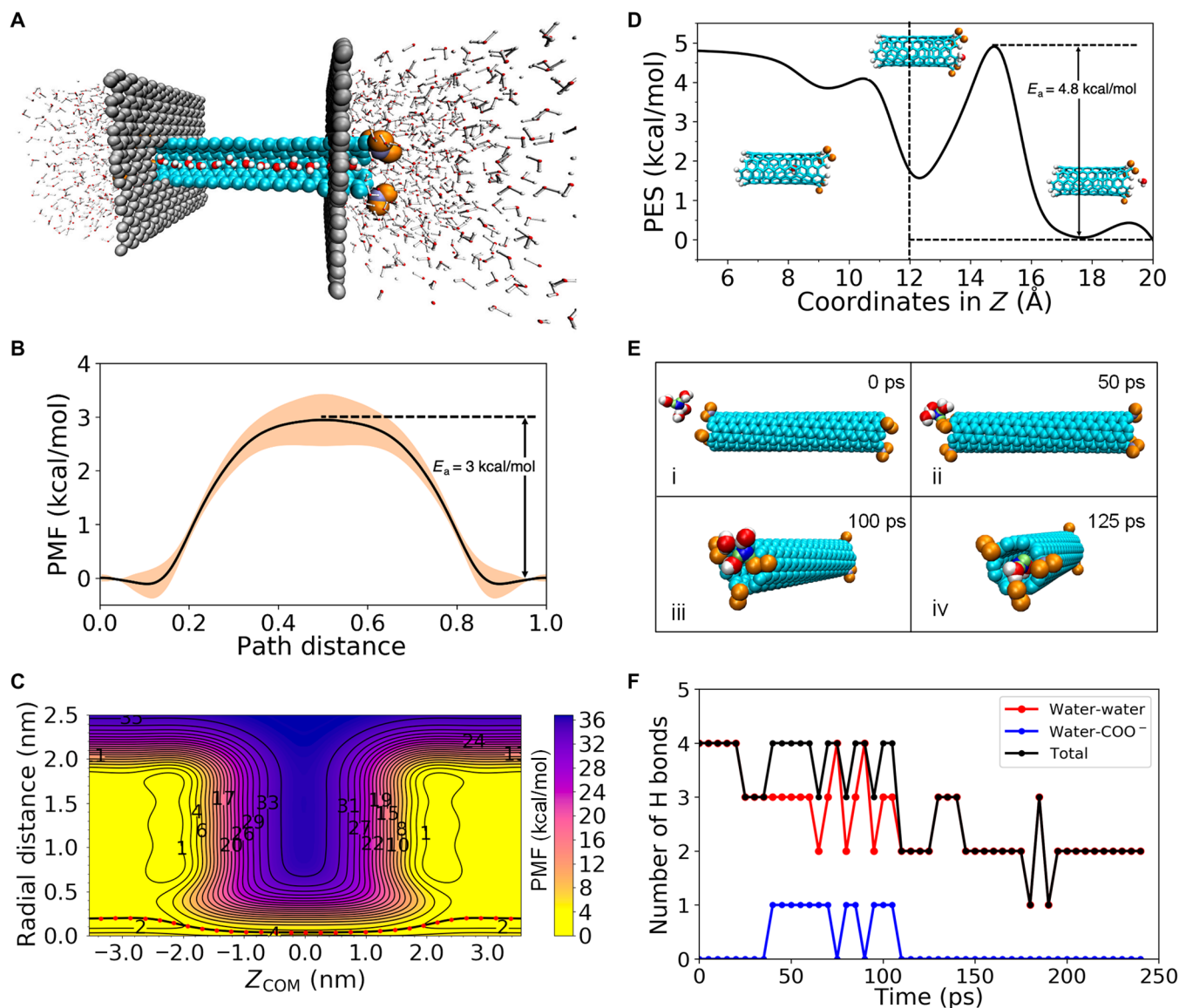


**Fig. 3. Simulation of water transport in CNTPs.** (A) Snapshot from a WT-MetaD simulation showing the model system consisting of two water reservoirs, two graphene sheets, and a CNT. (B) 1D PMF of a water molecule transporting through the CNTP with respect to the length of the minimum free energy path. “0” and “1” correspond to the bulk water found in two reservoirs, and “0.5” corresponds to the center of the CNTP. The error bars are estimated from the SD of three independent replicas. (C) 2D PMF of a water molecule transporting through the CNTP computed from an average of three independent simulations. The black line represents the minimum free energy path. (D) 1D free energy profile of a water molecule transporting through the CNTP as obtained from hybrid quantum-continuum simulations, where the interaction between the permeated water molecule and CNTP was explicitly described using DFT and the rest of the liquid was treated by an implicit solvation model (see Materials and Methods for more details). The vertical dashed line indicates the position of the CNTP entrance. PES, potential energy surface. (E) Snapshots from a WT-MetaD simulation showing the process of water entering the CNTP at different time points in the simulation. (F) Evolution of the total number of hydrogen bonds (black lines and markers) formed by a water molecule transitioning the CNTP. Water-water (red lines and markers) and water-COO<sup>-</sup> bonds (blue lines and markers) correspond to the number of hydrogen bonds formed with other water molecules and the COO<sup>-</sup> groups at the entrance of the CNTP.

negatively charged COO<sup>-</sup> groups at the pore mouth at neutral pH (16). This behavior also indicates that the counterion (Cl<sup>-</sup> anion) selectivity is the critical parameter that would determine the overall CNTP salt rejection and, thus, their performance in the reverse osmosis desalination applications. We quantified chloride ion transport through the CNTPs with an assay (Fig. 4A) that relied on the ability of those ions to cause collision quenching of fluorescence of halide-sensitive fluorophore lucigenin (21, 31). In these experiments,

we initiated the transport by mixing the solution of the lucigenin-encapsulating CNTP-LUVs with a chloride-containing buffer in a stopped-flow spectrometer mixer. To ensure the absence of the membrane potential, which could slow down the anion transport, we added K<sup>+</sup> ionophore, valinomycin, to the CNTP-LUVs. To avoid generating osmotically driven water fluxes in CNTPs, we have also balanced the osmotic pressure of the Cl<sup>-</sup> ions outside the vesicles with the equivalent concentration of NO<sub>3</sub><sup>-</sup> ions inside the vesicles.

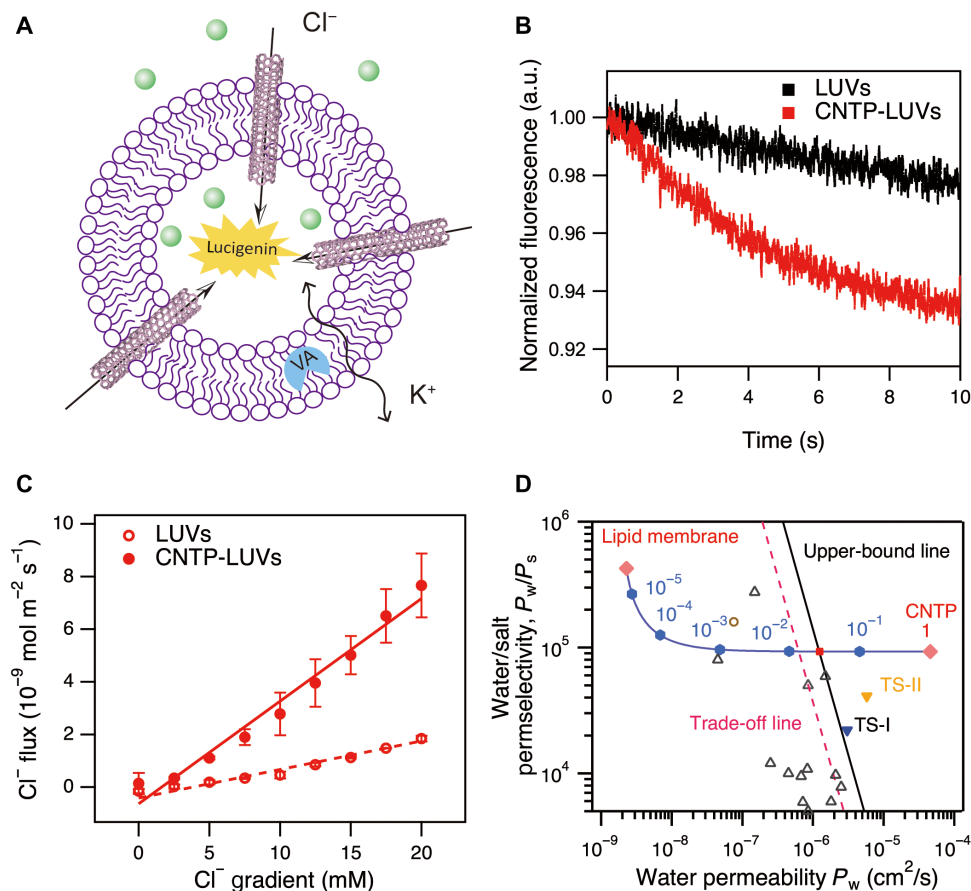


**Fig. 4. Cl<sup>-</sup> ion transport and water-salt permselectivity of CNTP.** (A) Schematic of the chloride ion permeation assay showing lucigenin dye encapsulated in a liposome and Cl<sup>-</sup> ion diffusion into the liposome through CNTP channels in the liposome wall. Valinomycin (VA) ionophore is added to the lipid bilayer to ensure that counterion (K<sup>+</sup>) transport does not impede anion diffusion. (B) Representative lucigenin fluorescence traces obtained in the Cl<sup>-</sup> permeability measurements for CNTPs-LUVs, which contained, on average, 10 CNTPs per vesicle, and control LUVs. In both experiments, vesicles were exposed to 15 mM Cl<sup>-</sup> gradient. (C) Chloride flux plotted as a function of chloride concentration gradient for CNTPs-LUVs and control LUVs. (D) Projected seawater desalination performance of composite lipid-CNTP (blue hexagon symbols) for different CNTP area fractions in the membrane (the corresponding numbers on the plot, where 0 corresponds to pure lipid membrane and 1 to pure CNTP). The performance of commercial desalination membranes (black open triangles), Turing-type polyamide membranes, TS-I and TS-II (solid inverted triangle), and graphene-nanomesh/single-walled CNT hybrid membrane (brown open circle) are adapted from (57–59). Dashed red and solid black lines indicate the trade-off line and upper-bound line (3, 60). TS, Turing structure.

The decay in lucigenin emission observed in the stopped-flow fluorescence signal traces (Fig. 4B) indicated that chloride ions were entering into the vesicle and provided a quantitative measurement of the chloride ion flux. When the LUV walls contained CNTP channels, chloride entry was faster than in the control experiment, indicating that CNTPs were transporting the chloride ion, albeit fairly slowly. The linear relationship between measured chloride flux and the applied concentration gradient (Fig. 4C) indicated that anion transport followed Fickian diffusion. After subtraction of the background LUV permeability, we calculated the unitary chloride permeability,  $P_s$ , for single CNTP at pH 7.5 as  $(2.48 \pm 0.31) \times 10^{-18}$  cm<sup>3</sup>/s. This value is quite small; for comparison, the Cl<sup>-</sup> channel of rat hippocampal neurons has a permeability of around  $2.5 \times 10^{-14}$  cm<sup>3</sup>/s, as calculated from conductance and Cl<sup>-</sup>/Na<sup>+</sup> selectivity (32).

When we combined the values of the measured chloride ion permeability of the CNTPs and their water permeability, we obtained a water-salt permselectivity,  $P_w/P_s$ , value of  $9.2 \times 10^4$ . To further refine the estimate for this key membrane performance parameter, we measured water and chloride permeability values using the same

batch of CNTPs, which helped us exclude the possible error from estimating the number of channels per vesicle (fig. S6). These measurements produced a similar  $P_w/P_s$  value of  $8.4 \times 10^4$ .

Significantly lower permeability of chloride ions compared with water is also consistent with our theoretical calculations. In particular, we found that the activation energy for Cl<sup>-</sup> transport through CNTPs obtained from WT-MetaD simulations is about 40 kcal/mol, i.e., an order magnitude higher than that of water (fig. S7). While these results point to a lower permeability of chloride ions compared with water, the activation energy of 40 kcal/mol obtained from force field simulations drastically overestimates the value of about 12.3 kcal/mol predicted from the  $P_w/P_s$  ratio using a simple transition state theory approach. On the other hand, we found that the use of a hybrid quantum-continuum approach that explicitly describes the ion-CNTP interaction at the DFT level of theory significantly improves the agreement with experimental results, yielding an activation energy of about 15 kcal/mol for chloride ion (fig. S8). The result indicates that the inclusion of polarization effects beyond a simple point-charge approximation that is often used in force field simulations is

important for an accurate estimate of the activation energy of ion permeation through CNTPs (33).

## DISCUSSION

The  $P_w/P_s$  values obtained in our studies are comparable to the typical  $10^5$  permselectivity values for the commercial TFC desalination membranes (4), indicating that CNTP channels could indeed provide viable performance for seawater desalination applications. Nevertheless, we note that this performance is still seven orders of magnitude lower than the projected performance of biomimetic membranes with aquaporin pores (4). It is worth noting that chloride ions are four orders of magnitude more permeable through lipid membrane than sodium ions (34), which would also contribute to the permselectivity gap between the membrane-based CNTPs and aquaporins, which have strong rejection of both types of ions.

To explore the potential performance on CNTP-based membranes for seawater desalination, we used our results to calculate the water permeability and water/salt permselectivity for different channel densities of lipid membranes (Fig. 4D) and compared these values with those of commercial water desalination membranes. These estimates indicate that CNTP membrane performance can indeed break the permeability/selectivity upper bound that limits the performance of TFC polymer membranes, as long as the channel area density exceeds a relatively modest 2.7% value. Besides increasing pore density, it is also clear that another way to enhance membrane performance would be to improve CNTP permselectivity. A straightforward pathway to enhance permselectivity of a single-file water channel would be to reduce its size (35). For example, pillar[5]arene (PAP[5]) channels (36) with a pore size of around 4.7 Å still have some ion permeability (8), whereas narrower 3-Å aquaporin pores completely reject ions (6). The narrowest chirality of single-walled CNT that can be separated from commercially available source is (6, 4) (37), which has an effective diameter of ca. 4 Å (the value taken from nominal 6.8-Å diameter and adjusted for the van der Waals diameter of carbon atoms). At this size, a CNTP channel is still likely to transport some ions. Thus, further improvements of the salt rejection of CNTPs may require further functionalization (38) of the CNTP pore mouth or their sidewalls.

Other potential obstacles include the mechanical stability of membranes containing CNT pores and scaling up the membrane areas to values relevant to water purification applications. Any membrane using short CNT pores will require a robust support to ensure that it can withstand pressure drops required for reverse osmosis desalination. Even though vesicle fusion could produce large-area membranes (39), the fidelity of this process needs further improvement. Block copolymer membranes incorporating CNT pores (40) could provide a more robust composite than lipid bilayers and UV or chemical cross-linking could further improve mechanical properties. Recent reports on composite polymer membranes incorporating synthetic PAP[5] nanochannels (41) and membrane proteins (42) also demonstrate the potential routes to scalable biomimetic membranes.

Our results show that, in addition to being fast water transporters, CNTPs have strong rejection of chloride anions with an overall channel water-salt permselectivity that is comparable to that of commercial desalination membranes. Temperature-resolved transport measurements and MD simulations show that the water that enters into the CNTP channel encounters a low energy barrier of ca. 5.3 kcal/mol. This behavior is also consistent with the behavior

observed for other single-file water channels. These observations establish the possibility of using narrow CNT pores for water desalination and point to the improvements that still need to be made for these pores to realize their full potential.

## MATERIALS AND METHODS

### Materials and LUV preparation

DOPC was obtained from Avanti Polar Lipids. 5(6)-CF, Hepes, sodium chloride, Hepes potassium salt, potassium chloride, potassium nitrate, cholesterol, *N,N'*-dimethyl-9,9'-biacridinium dinitrate (lucigenin), sucrose, valinomycin, and single-walled CNTs (catalog no. 773735) were obtained from Sigma-Aldrich Inc. The 0.8-nm-diameter CNTPs were prepared and purified using previously published protocols (43). As described previously, the CNTP/vesicle ratio or incorporation efficiency was determined by dividing measured proton permeability of CNTP-LUVs by the unitary proton permeabilities of CNTPs (43).

To prepare the LUVs DOPC or DOPC/cholesterol (9:1, mol/mol), lipid in chloroform was aliquoted (2 mg) into glass vials, and the solvent was evaporated under a stream of air and then further dried at least 2 hours in a vacuum desiccator chamber. One milliliter of pH 7.5 buffer was added to the dried lipid film to obtain a suspension. To incorporate CNTPs into the liposomes, we first dried 0.25 to 1 ml of the appropriate CNTP solution overnight in a vacuum desiccator to remove the solvent. The dried CNTP film was hydrated with 1 ml of pH 7.5 buffer and bath sonicated for 30 s to ensure that the film is completely solubilized and detached from the glass vial. This solution was subsequently used to hydrate a 2-mg lipid film and bath sonicated to mix thoroughly. The liposome solutions were hydrated at room temperature for 30 min. To ensure formation of LUVs or CNTP-LUVs, the samples underwent 10 cycles of freeze-thaw treatment where the liposomes were flash frozen in liquid nitrogen and subsequently thawed at 50°C. The LUVs or CNTP-LUVs were then extruded at least 21 times through 200-nm pore-sized polycarbonate track-etched membranes using a mini extruder (Avanti Polar Lipids). To remove extravesicular CF from the liposome solution, size exclusion chromatography with a column containing Sepharose CL-6B (Sigma-Aldrich) was performed. Fractions were collected in a 96-well plate, and fractions containing liposomes were pooled. Average vesicle hydrodynamic radius was determined by dynamic light scattering using a Zetasizer Nano ZS90 (Malvern Instruments).

### CNTP water permeability measurements

Water permeabilities of CNTP-LUVs or pure LUVs were measured using a stopped-flow fluorometer (SFM2000; MOS-200, Bio-Logic) equipped with a single band-pass emission filter (Chroma Technology; center wavelength, 510 nm; full bandwidth, 20 nm). The excitation wavelength was set at 492 nm. LUVs were prepared with an intravesicular solution of 20 mM Hepes K, 85 mM NaCl, 15 mM CF (pH 7.5), and buffer exchanged into an isosmotic solution of 20 mM Hepes K and 100 mM NaCl (pH 7.5). During experiments, LUV solutions were rapidly mixed 1:4 or 1:1 with a hypertonic solution containing 20 mM Hepes K, 100 mM NaCl, and 200 mM solute (NaCl or sucrose) (pH 7.5). Fluorescence intensity changed due to self-quenching of CF at high concentrations was recorded. At least three traces were averaged for each data point. The membrane water permeability,  $P_b$ , was determined using published protocols

(4, 22, 23) by, first, applying the linear conversion from relative fluorescence to relative volume and then iteratively solving the water permeability equation. Briefly, the time trace of the decrease in fluorescence was fitted to a single exponential curve. The osmotic water permeability,  $P_f$ , was calculated from the numerical fit of the resulting single exponential curve to the water permeability equation (Eq. 1; see also fig. S4)

$$\frac{dV_r(t)}{dt} = P_f \times \frac{A}{V_0} \times V_w \times \left( \frac{C_{in}}{V_r(t)} - C_{out} \right) \quad (1)$$

where  $V_r(t)$  is the relative volume of the vesicle at time  $t$ ,  $P_f$  is the osmotic water permeability coefficient,  $A/V_0$  is the surface area-to-volume ratio of a vesicle,  $C_{in}$  and  $C_{out}$  are initial solute concentrations inside and outside the vesicle, respectively, and  $V_w$  is the molar volume of water. We also compared the water permeability coefficients obtained with this procedure with the values determined with a different protocol (44) that computes permeabilities directly from the time constants and found that both approaches give permeability values that differ by less than 10% (with the second approach producing systematically higher values). The unitary water permeability  $P_w$  of CNTPs was calculated using the following expression after subtracting the background vesicle permeability

$$P_w = (P_f^{\text{CNTP-LUVs}} - P_f^{\text{LUVs}}) \times \frac{A}{N} \quad (2)$$

where  $A$  is the surface area of the CNTP-LUVs, and  $N$  is the average number of CNTPs in the vesicle.

### Activation energy measurements

To determine activation energies for water transport, we repeated water permeability measurements for LUVs and CNTP-LUVs at different temperatures, as indicated in the main text. For these experiments, the solution reservoirs and the measurement cell of the stopped-flow instrument were maintained at a preset temperature by a thermal circulator, and the exact temperature of the sample was determined by a temperature probe connecting to the measurement cell.

### Chloride permeability measurements

Measurements of chloride permeability of both control blank LUVs and CNTP-LUVs were performed in the same stopped-flow fluorescence spectrometer setup. Excitation wavelength was set at 455 nm, and the detection channel was equipped with 488-nm EdgeBasic long-pass edge filter. To initiate  $\text{Cl}^-$  ion transport across the membrane, LUVs were rapidly exposed to different gradients of chloride in the stopped-flow measurement cell. For example, to impose 20 mM  $\text{Cl}^-$  gradient, 75  $\mu\text{l}$  of vesicle samples (pH 7.5, 10 mM Hepes, and 100 mM  $\text{KNO}_3$ ) were mixed with 75  $\mu\text{l}$  of  $\text{Cl}^-$ -containing buffer (pH 7.5, 10 mM Hepes, 40 mM KCl, and 60 mM  $\text{KNO}_3$ ). Valinomycin was added to the vesicle samples beforehand to mitigate charge imbalance across the membrane and to prevent the underestimation of target anions permeability due to electrical potential developed on the membrane. The final concentration of valinomycin in the mixed solutions was 10  $\mu\text{M}$ .  $\text{NO}_3^-$  ions were used as counterions of halide anions for balancing osmotic pressure across the vesicular membranes. All measurements were performed at 23°C. More than seven individual traces

were recorded for each value of  $\text{Cl}^-$  gradient, and the averaged traces were used for analysis.

### MD simulations

All-atom MD simulations were carried out using the LAMMPS package (45) and CHARMM force fields (46). A (6,5) CNT with 0.75-nm diameter and 4-nm length was placed between two graphene sheets that mimic the lipid bilayer structure of liposomes in experiments (see Fig. 3A). The CNTP was modeled as a rigid and charged neutral structure, and each entrance was functionalized with three carboxylate groups ( $\text{COO}^-$ ). Both sides of the simulation box were solvated by approximately 2-nm-thick layers of TIP3P water, and  $\text{K}^+$  and  $\text{Cl}^-$  ions were randomly inserted to neutralize the system. The system was first energy minimized and then equilibrated for 1 ns under NPT ensemble at  $T = 298.15$  K and  $P = 1$  atm.

To determine the activation energy of water and ion permeation through the CNT, WT-MetaD (27) was used to determine the 2D PMF. In the MetaD approach (47), a history-dependent bias energy in the form of Gaussian potential is added to the Hamiltonian of the system through predetermined collective variables (CVs) to bias the normal evolution of the system. In this way, sampling of rare events is accelerated by discouraging the system from revisiting the previously visited regions in the free energy landscape. In the conventional MetaD approach, the height of the Gaussian remains constant during the simulation that may result in false convergence or destabilization of the system (48). WT-MetaD used here resolves this issue by introducing a time-dependent bias potential that results in asymptotic convergence of the PMF (49).

The 2D PMF for water and ion transport was evaluated by averaging the results from three independent ~400-ns WT-MetaD simulations. A 1D PMF was then obtained by calculating the minimum free energy path on the 2D PMF. In all simulations, two CVs were used to facilitate PMF convergence (50, 51), including the center of mass distance between the oxygen atom of the water molecule and CNT along the direction of the tube axis, and the radial position of the water molecule with respect to the center of CNT. Hydrogen bond analysis was based on a simple geometrical criterion adapted from (52).

In addition to WT-MetaD simulations with classical force fields, we used a hybrid quantum-continuum approach that combines DFT with implicit solvation model to further refine the activation energy of water and ion transport through the CNTP (30). Here, the water molecule and chloride ion, as well as the CNTP, were explicitly described using DFT with the van der Waals density functional (vdW-DF2) (53). As discussed in our previous study (33), the hybrid quantum-continuum approach goes beyond a simple point-charge approximation that is often used in conventional classical simulations, thereby providing a more realistic description of the water-CNTP and ion-CNTP interactions. In these calculations, ultrasoft pseudopotentials were used for the description of the interaction between valence electrons and ionic cores (54); in addition, the electronic wave function and charge density were expanded in a plane-wave basis set truncated at the cutoff energies of 40 and 320 rydberg, respectively. The implicit solvent in these calculations was described in the framework of the reference interaction site method (RISM), where atomic charges and Lennard-Jones potentials of the solvent and ions were described through the optimized potentials for liquid simulations of all-atom force fields (55). All the hybrid quantum-continuum calculations were carried out with the Quantum ESPRESSO package (56).

## SUPPLEMENTARY MATERIALS

Supplementary material for this article is available at <http://advances.sciencemag.org/cgi/content/full/6/38/eaba9966/DC1>

[View/request a protocol for this paper from Bio-protocol.](#)

## REFERENCES AND NOTES

- M. A. Shannon, P. W. Bohn, M. Elimelech, J. G. Georgiadis, B. J. Mariñas, A. M. Mayes, Science and technology for water purification in the coming decades. *Nature* **452**, 301–310 (2008).
- J. R. Werber, C. O. Osuji, M. Elimelech, Materials for next-generation desalination and water purification membranes. *Nat. Rev. Mat.* **1**, 16018 (2016).
- G. M. Geise, H. B. Park, A. C. Sagle, B. D. Freeman, J. E. McGrath, Water permeability and water/salt selectivity tradeoff in polymers for desalination. *J. Membr. Sci.* **369**, 130–138 (2011).
- J. R. Werber, M. Elimelech, Permselectivity limits of biomimetic desalination membranes. *Sci. Adv.* **4**, eaar8266 (2018).
- J. R. Werber, A. Deshmukh, M. Elimelech, The critical need for increased selectivity, not increased water permeability, for desalination membranes. *Environ. Sci. Technol. Lett.* **3**, 112–120 (2016).
- P. Agre, L. S. King, M. Yasui, W. B. Guggino, O. P. Ottersen, Y. Fujiyoshi, A. Engel, S. Nielsen, Aquaporin water channels – from atomic structure to clinical medicine. *J. Physiol.* **542**, 3–16 (2002).
- M. Barboiu, Artificial water channels – incipient innovative developments. *Chem. Commun.* **52**, 5657–5665 (2016).
- W. Song, C. Lang, Y.-x. Shen, M. Kumar, Design considerations for artificial water channel-based membranes. *Annu. Rev. Mat. Res.* **48**, 57–82 (2018).
- K. Falk, F. Sedlmeier, L. Joly, R. R. Netz, L. Bocquet, Molecular origin of fast water transport in carbon nanotube membranes: Superlubricity versus curvature dependent friction. *Nano Lett.* **10**, 4067–4073 (2010).
- G. Hummer, J. C. Rasaiah, J. P. Noworyta, Water conduction through the hydrophobic channel of a carbon nanotube. *Nature* **414**, 188–190 (2001).
- S. Joseph, N. R. Aluru, Why are carbon nanotubes fast transporters of water? *Nano Lett.* **8**, 452–458 (2008).
- T. A. Pascal, W. A. Goddard, Y. Jung, Entropy and the driving force for the filling of carbon nanotubes with water. *Proc. Natl. Acad. Sci. U.S.A.* **108**, 11794–11798 (2011).
- M. Majumder, N. Chopra, R. Andrews, B. J. Hinds, Enhanced flow in carbon nanotubes. *Nature* **438**, 44 (2005).
- J. K. Holt, H. G. Park, Y. Wang, M. Stadermann, A. B. Artyukhin, C. P. Grigoropoulos, A. Noy, O. Bakajin, Fast mass transport through sub-2-nanometer carbon nanotubes. *Science* **312**, 1034–1037 (2006).
- E. Secchi, S. Marbach, A. Niguès, D. Stein, A. Siria, L. Bocquet, Massive radius-dependent flow slippage in carbon nanotubes. *Nature* **537**, 210–213 (2016).
- R. H. Tunuguntla, R. Y. Henley, Y.-C. Yao, T. A. Pham, M. Wanunu, A. Noy, Enhanced water permeability and tunable ion selectivity in subnanometer carbon nanotube porins. *Science* **357**, 792–796 (2017).
- B. Corry, Designing carbon nanotube membranes for efficient water desalination. *J. Phys. Chem. B* **112**, 1427–1434 (2008).
- H. J. Kim, K. Choi, Y. Baek, D.-G. Kim, J. Shim, J. Yoon, J.-C. Lee, High-performance reverse osmosis CNT/polyamide nanocomposite membrane by controlled interfacial interactions. *ACS Appl. Mater. Interfaces* **6**, 2819–2829 (2014).
- J. Geng, K. Kim, J. Zhang, A. Escalada, R. Tunuguntla, L. R. Comolli, F. I. Allen, A. V. Shnyrova, K. R. Cho, D. Munoz, Y. M. Wang, C. P. Grigoropoulos, C. M. Ajo-Franklin, V. A. Frolov, A. Noy, Stochastic transport through carbon nanotubes in lipid bilayers and live cell membranes. *Nature* **514**, 612–615 (2014).
- A. Horner, F. Zoicher, J. Preiner, N. Ollinger, C. Siligan, S. A. Akimov, P. Pohl, The mobility of single-file water molecules is governed by the number of H-bonds they may form with channel-lining residues. *Sci. Adv.* **1**, e1400083 (2015).
- A. S. Verkman, Optical methods to measure membrane transport processes. *J. Membr. Biol.* **148**, 99–110 (1995).
- M. L. Zeidel, S. V. Ambudkar, B. L. Smith, P. Agre, Reconstitution of functional water channels in liposomes containing purified red cell CHIP28 protein. *Biochemistry* **31**, 7436–7440 (1992).
- J. C. Mathai, S. Tristram-Nagle, J. F. Nagle, M. L. Zeidel, Structural determinants of water permeability through the lipid membrane. *J. Gen. Physiol.* **131**, 69–76 (2008).
- A. Horner, P. Pohl, Comment on “enhanced water permeability and tunable ion selectivity in subnanometer carbon nanotube porins”. *Science* **359**, eaap9173 (2018).
- A. Horner, P. Pohl, Single-file transport of water through membrane channels. *Faraday Discuss.* **209**, 9–33 (2018).
- K. Olbrich, W. Rawicz, D. Needham, E. Evans, Water permeability and mechanical strength of polyunsaturated lipid bilayers. *Biophys. J.* **79**, 321–327 (2000).
- A. Barducci, G. Bussi, M. Parrinello, Well-tempered metadynamics: A smoothly converging and tunable free-energy method. *Phys. Rev. Lett.* **100**, 020603 (2008).
- C. Y. Won, S. Joseph, N. R. Aluru, Effect of quantum partial charges on the structure and dynamics of water in single-walled carbon nanotubes. *J. Chem. Phys.* **125**, 114701 (2006).
- C. Zhang, J. Wu, G. Galli, F. Gygi, Structural and vibrational properties of liquid water from van der Waals density functionals. *J. Chem. Theory Comput.* **7**, 3054–3061 (2011).
- S. Nishihara, M. Otani, Hybrid solvation models for bulk, interface, and membrane: Reference interaction site methods coupled with density functional theory. *Phys. Rev. B* **96**, 115429 (2017).
- J. Biwersi, B. Tulk, A. S. Verkman, Long-wavelength chloride-sensitive fluorescent indicators. *Anal. Biochem.* **219**, 139–143 (1994).
- F. Franciolini, W. Nonner, Anion and cation permeability of a chloride channel in rat hippocampal neurons. *J. Gen. Physiol.* **90**, 453–478 (1987).
- C. Zhan, M. R. Cerón, S. A. Hawks, M. Otani, B. C. Wood, T. A. Pham, M. Stadermann, P. G. Campbell, Specific ion effects at graphitic interfaces. *Nat. Commun.* **10**, 4858 (2019).
- S. Paula, A. G. Volkov, D. W. Deamer, Permeation of halide anions through phospholipid bilayers occurs by the solubility-diffusion mechanism. *Biophys. J.* **74**, 319–327 (1998).
- V. Freger, Selectivity and polarization in water channel membranes: Lessons learned from polymeric membranes and CNTs. *Faraday Discuss.* **209**, 371–388 (2018).
- Y.-X. Shen, W. Si, M. Erbakan, K. Decker, R. De Zorzi, P. O. Saboe, Y. J. Kang, S. Majid, P. J. Butler, T. Walz, A. Aksimentiev, J.-I. Hou, M. Kumar, Highly permeable artificial water channels that can self-assemble into two-dimensional arrays. *Proc. Natl. Acad. Sci. U.S.A.* **112**, 9810–9815 (2015).
- H. Liu, D. Nishide, T. Tanaka, H. Kataura, Large-scale single-chirality separation of single-wall carbon nanotubes by simple gel chromatography. *Nat. Commun.* **2**, 309 (2011).
- R. H. Tunuguntla, A. Y. Hu, Y. Zhang, A. Noy, Impact of PEG additives and pore rim functionalization on water transport through sub-1 nm carbon nanotube porins. *Faraday Discuss.* **209**, 359–369 (2018).
- Y. Kaufman, A. Berman, V. Freger, Supported lipid bilayer membranes for water purification by reverse osmosis. *Langmuir* **26**, 7388–7395 (2010).
- J. R. Sanborn, X. Chen, Y.-C. Yao, J. A. Hammons, R. H. Tunuguntla, Y. Zhang, C. C. Newcomb, J. A. Soltis, J. J. De Yoreo, A. Van Buuren, A. N. Parikh, A. Noy, Carbon nanotube porins in amphiphilic block copolymers as fully synthetic mimics of biological membranes. *Adv. Mater.* **30**, 1803355 (2018).
- Q. Li, X. Li, L. Ning, C.-H. Tan, Y. Mu, R. Wang, L. Ning, Hyperfast water transport through biomimetic nanochannels from peptide-attached (pR)-pillar[5]arene. *Small* **15**, e1804678 (2019).
- Y.-M. Tu, W. Song, T. Ren, Y.-X. Shen, R. Chowdhury, P. Rajapaksha, T. E. Culp, L. Samineni, C. Lang, A. Thokkadam, D. Carson, Y. Dai, A. Mukhtar, M. Zhang, A. Parshin, J. N. Sloand, S. H. Medina, M. Grzelakowski, D. Bhattacharya, W. A. Phillip, E. D. Gomez, R. J. Hickey, Y. Wei, M. Kumar, Rapid fabrication of precise high-throughput filters from membrane protein nanosheets. *Nat. Mater.* **19**, 347–354 (2020).
- R. H. Tunuguntla, A. Escalada, V. A. Frolov, A. Noy, Synthesis, lipid membrane incorporation, and ion permeability testing of carbon nanotube porins. *Nat. Protoc.* **11**, 2029–2047 (2016).
- C. Hanneschläger, T. Barta, C. Siligan, A. Horner, Quantification of water flux in vesicular systems. *Sci. Rep.* **8**, 8516 (2018).
- S. Plimpton, Fast parallel algorithms for short-range molecular dynamics. *J. Comput. Phys.* **117**, 1–19 (1995).
- A. D. MacKerell, D. Bashford, M. Bellott, R. L. Dunbrack, J. D. Evanseck, M. J. Field, S. Fischer, J. Gao, H. Guo, S. Ha, D. Joseph-McCarthy, L. Kuchnir, K. Kuczera, F. T. Lau, C. Mattos, S. Michnick, T. Ngo, D. T. Nguyen, B. Prodhom, W. E. Reiher, B. Roux, M. Schlenkerich, J. C. Smith, R. Stote, J. Straub, M. Watanabe, J. Wiórkiewicz-Kuczera, D. Yin, M. Karplus, All-atom empirical potential for molecular modeling and dynamics studies of proteins. *J. Phys. Chem. B* **102**, 3586–3616 (1998).
- A. Laio, M. Parrinello, Escaping free-energy minima. *Proc. Natl. Acad. Sci. U.S.A.* **99**, 12562–12566 (2002).
- R. Sun, J. F. Dama, J. S. Tan, J. P. Rose, G. A. Voth, Transition-tempered metadynamics is a promising tool for studying the permeation of drug-like molecules through membranes. *J. Chem. Theory Comput.* **12**, 5157–5169 (2016).
- J. F. Dama, M. Parrinello, G. A. Voth, Well-tempered metadynamics converges asymptotically. *Phys. Rev. Lett.* **112**, 240602 (2014).
- F. Aydin, R. Sun, J. M. J. Swanson, Mycolactone toxin membrane permeation: Atomistic versus Coarse-Grained MARTINI Simulations. *Biophys. J.* **117**, 87–98 (2019).
- R. Sun, Y. Han, J. M. J. Swanson, J. S. Tan, J. P. Rose, G. A. Voth, Molecular transport through membranes: Accurate permeability coefficients from multidimensional potentials of mean force and local diffusion constants. *J. Chem. Phys.* **149**, 072310 (2018).

52. A. Nag, D. Chakraborty, A. Chandra, Effects of ion concentration on the hydrogen bonded structure of water in the vicinity of ions in aqueous NaCl solutions. *J. Chem. Sci.* **120**, 71–77 (2008).
53. M. Dion, H. Rydberg, E. Schröder, D. C. Langreth, B. I. Lundqvist, Van der Waals density functional for general geometries. *Phys. Rev. Lett.* **92**, 246401 (2004).
54. D. Vanderbilt, Soft self-consistent pseudopotentials in a generalized eigenvalue formalism. *Phys. Rev. B* **41**, 7892–7895 (1990).
55. W. L. Jorgensen, J. Tirado-Rives, The OPLS [optimized potentials for liquid simulations] potential functions for proteins, energy minimizations for crystals of cyclic peptides and crambin. *J. Am. Chem. Soc.* **110**, 1657–1666 (1988).
56. P. Giannozzi, S. Baroni, N. Bonini, M. Calandra, R. Car, C. Cavazzoni, D. Ceresoli, G. L. Chiarotti, M. Cococcioni, I. Dabo, A. D. Corso, S. de Gironcoli, S. Fabris, G. Fratesi, R. Gebauer, U. Gerstmann, C. Gougoussis, A. Kokalj, M. Lazzeri, L. Martin-Samos, N. Marzari, F. Mauri, R. Mazzarello, S. Paolini, A. Pasquarello, L. Paulatto, C. Sbraccia, S. Scandolo, G. Sclauzero, A. P. Seitsonen, A. Smogunov, P. Umari, R. M. Wentzcovitch, QUANTUM ESPRESSO: A modular and open-source software project for quantum simulations of materials. *J. Phys. Condens. Matter* **21**, 395502 (2009).
57. C. Klaysom, T. Y. Cath, T. Depuydt, I. F. J. Vankelecom, Forward and pressure retarded osmosis: Potential solutions for global challenges in energy and water supply. *Chem. Soc. Rev.* **42**, 6959–6989 (2013).
58. Z. Tan, S. Chen, X. Peng, L. Zhang, C. Gao, Polyamide membranes with nanoscale Turing structures for water purification. *Science* **360**, 518–521 (2018).
59. Y. Yang, X. Yang, L. Liang, Y. Gao, H. Cheng, X. Li, M. Zou, R. Ma, Q. Yuan, X. Duan, Large-area graphene-nanomesh/carbon-nanotube hybrid membranes for ionic and molecular nanofiltration. *Science* **364**, 1057–1062 (2019).
60. N. Y. Yip, M. Elimelech, Performance limiting effects in power generation from salinity gradients by pressure retarded osmosis. *Environ. Sci. Technol.* **45**, 10273–10282 (2011).

**Acknowledgments:** Work at the Lawrence Livermore National Laboratory was performed under the auspices of the U.S. Department of Energy under Contract DE-AC52-07NA27344. Work at the Molecular Foundry was supported by the Office of Science, Office of Basic Energy Sciences, of the U.S. Department of Energy under contract no. DE-AC02-05CH11231. **Funding:** This work was supported as part of the Center for Enhanced Nanofluidic Transport (CENT), an Energy Frontier Research Center funded by the U.S. Department of Energy, Office of Science, Basic Energy Sciences under award no. DE-SC0019112. Z.L. is supported by the Scientific Research Foundation of Graduate School of Southeast University (grant no. YBJJ1802) and the Postgraduate Research and Practice Innovation Program of Jiangsu Province (grant no. KYCX18\_0067) and acknowledges financial support from the China Scholarship Council (CSC 201806090020). Computational support was from the LLNL Grand Challenge Program. **Author contributions:** Y.L., Z.L., and A.N. designed the experiments. Y.L., Z.L., J.Q., X.C., and Y.-C.Y. performed the experiments. F.A., C.Z., and T.A.P. designed and performed computer simulations. Y.L., Z.L., F.A., T.A.P., and A.N. wrote the paper. All authors commented on the results and participated in the editing of the manuscript. **Competing interests:** The authors declare that they have no competing interests. **Data and materials availability:** All data needed to evaluate the conclusions in the paper are present in the paper and/or the Supplementary Materials. Additional data related to this paper may be requested from the authors. Data presented in this work are available at DOI: 10.6084/m9.figshare.12032286 or from the corresponding author upon request.

Submitted 25 January 2020

Accepted 29 July 2020

Published 16 September 2020

10.1126/sciadv.aba9966

**Citation:** Y. Li, Z. Li, F. Aydin, J. Quan, X. Chen, Y.-C. Yao, C. Zhan, Y. Chen, T. A. Pham, A. Noy, Water-ion permselectivity of narrow-diameter carbon nanotubes. *Sci. Adv.* **6**, eaba9966 (2020).

## Water-ion permselectivity of narrow-diameter carbon nanotubes

Yuhao Li, Zhongwu Li, Fikret Aydin, Jana Quan, Xi Chen, Yun-Chiao Yao, Cheng Zhan, Yunfei Chen, Tuan Anh Pham and Aleksandr Noy

*Sci Adv* **6** (38), eaba9966.  
DOI: 10.1126/sciadv.aba9966

### ARTICLE TOOLS

<http://advances.sciencemag.org/content/6/38/eaba9966>

### SUPPLEMENTARY MATERIALS

<http://advances.sciencemag.org/content/suppl/2020/09/14/6.38.eaba9966.DC1>

### REFERENCES

This article cites 60 articles, 11 of which you can access for free  
<http://advances.sciencemag.org/content/6/38/eaba9966#BIBL>

### PERMISSIONS

<http://www.sciencemag.org/help/reprints-and-permissions>

Use of this article is subject to the [Terms of Service](#)

---

*Science Advances* (ISSN 2375-2548) is published by the American Association for the Advancement of Science, 1200 New York Avenue NW, Washington, DC 20005. The title *Science Advances* is a registered trademark of AAAS.

Copyright © 2020 The Authors, some rights reserved; exclusive licensee American Association for the Advancement of Science. No claim to original U.S. Government Works. Distributed under a Creative Commons Attribution NonCommercial License 4.0 (CC BY-NC).